International Journal of Heat and Mass Transfer 140 (2019) 777–785

Contents lists available at ScienceDirect

International Journal of Heat and Mass Transfer

journal homepage: www.elsevier.com/locate/ijhmt

Designing air-independent slippery rough surfaces for condensation

Gaurav Kumar Sirohia, Xianming Dai *

Department of Mechanical Engineering, The University of Texas at Dallas, Richardson, TX 75080, USA

ARTICLE INFO

Article history:
Received 7 March 2019
Received in revised form 9 June 2019
Accepted 10 June 2019
Available online 19 June 2019

Keywords:
Condensation
Nucleation
Liquid repellency
Superhydrophobic surface
Slippery rough surface

ABSTRACT

Enhancing condensation heat transfer is significant for power generation, heat exchangers, water harvesting, and air-conditioning. While superhydrophobic surfaces (SHS) are widely studied for condensation, this type of surface suffers from several weaknesses: (1) the hydrophobic surface chemistry does not favor nucleation, (2) the air lubricant has poor thermal conductivity, and (3) the air pocket may be displaced at an elevated humidity or subcooling. Patterned SHS can enhance vapor nucleation in the hydrophilic domains, but the superhydrophobic domains still rely on the air lubricant, resulting in the same weakness as SHS. Recently, the liquid infused surfaces have been developed by replacing the air lubricant with liquid lubricant, leading to more robust lubrication for liquid repellency. However, the original design of liquid infused surfaces shows a flat lubricant-water interface, which cannot provide a large contact area for heat transfer. Here, we successfully designed and manufactured the air-independent slippery rough surfaces (SRS) by conformal liquid lubrication on the rough solid surfaces. The surface chemistry of the SRS is governed by the liquid lubricant, not the solid textures, and the roughness is determined by the lubricated microtextures. Droplets are highly mobile on this air-independent slippery rough surface in the absence of air lubricant. Our comprehensive models provide rational design and optimization for the air-independent slippery rough surface that is highly desired in condensation heat transfer.

1. Introduction

Vapor condensation has a broad range of applications in power generation, heat exchangers, water harvesting, heat pipe, and air-conditioning [1,2]. There are two types of condensation modes: filmwise condensation and dropwise condensation. Dropwise condensation shows a 10 times lager heat transfer coefficient than filmwise condensation [3], because the condensate can be rapidly removed from the condensing surface, giving a small thermal resistance. Therefore, a super liquid-repellent surface is good for droplet removal and condensation enhancement. In nature, the lotus leaf inspired superhydrophobic surfaces (SHS) have micro/nanostructures and hydrophobic surface chemistry, so water droplets rest on the surface textures in a non-wetting state [4,5]. Superhydrophobic surfaces are air dependent as they rely on air gaps between the micro/nanostructures [6]. The air gaps can reduce the contact area between liquid droplets and the surface textures, resulting in reduced surface-droplet adhesion forces. When multiple droplets coalesce, the surface energy is converted to kinetic energy, leading to droplet jump. The effective removal of water droplets on SHS reduces the thermal resistance and significantly enhances condensation.

Although tremendous efforts have been made to create the lotus leaf inspired SHS for liquid repellency [7–11], recent studies have shown that SHS may lose the water repellency at a high subcooling even when high-quality nanowires are used [10]. The liquid repellency can be further improved by using three-dimensional superhydrophobic nanowires [12], but the condensation heat transfer coefficient is small owing to the ultra-low thermal conductivity of air (0.026 W/m K), and the low surface tension liquids cannot be repelled. This is because SHS rely on air as the lubricant so that the liquid droplet is partially floating on air. Researchers have developed the reentrant [13] and doubly reentrant structures [14] to improve the robustness of liquid repellency even to highly wetting liquids. However, the air layer can be displaced at a high subcooling because the nucleation starts form the nanoscale droplet [15]. Once the air is displaced, droplets transition from the Cassie state to the Wenzel state. In particular, the low surface tension fluids are likely to wet the entire rough surfaces. In addition, the vapor can nucleate to form nanodroplets within the surface textures, leading to direct wetting in the Wenzel state [16]. This type of Wenzel state droplets are strongly pinned on the surfaces. Researchers have tried to induce the wetting to

* Corresponding author.
E-mail address: Dai@utdallas.edu (X. Dai).

https://doi.org/10.1016/j.ijheatmasstransfer.2019.06.035
0017-9310/

non-wetting transitions on SHS [17–19], but those technologies can hardly be implemented in condensation. To date, robust SHS rely on hydrophobic surface coatings, which do not favor condensation nucleation. The weaknesses of SHS include: (1) the hydrophobic surface does not favor nucleation, (2) the air layer has a poor thermal conductivity, and (3) the air layer may be displaced at an elevated humidity or subcooling.

Thus, patterned SHS with hydrophilic domains have been developed to enhance nucleation [20–26]. Hydrophilic surfaces possess larger adhesion forces than hydrophobic surfaces when interacting with water droplets. Thus, the nucleation is enhanced, and the patterned SHS can delay the Cassie to Wenzel transition [25]. Nonetheless, the patterned SHS is also dependent on the air lubricant so the weaknesses of SHS are not circumvented. Recently, a patterned surface that combines hydrophilic and superhydrophilic domains is developed to facilitate dropwise condensation on the hydrophilic domains, and remove the condensate rapidly via the superhydrophilic domains [27]. This patterned superhydrophilic surface is not limited by the known shortcomings of hydrophobic chemistries, but the water-solid interface is not slippery.

To resolve the droplet mobility issue on the air-dependent superhydrophobic areas, a liquid repellent surface modeled after the slippery rim of the *Nepenthes* pitcher plant has been developed. This surface, known as slippery liquid-infused porous surfaces (SLIPS) or liquid infused surfaces [28–31], has a homogeneous and molecularly-smooth interface made by fully infusing a textured surface with hydrophobic liquid lubricant. The perfluorinated liquid infused surfaces showed an approximately 100% increase of heat transfer coefficient compared to the state-of-the-art dropwise condensation surfaces [9]. However, the perfluorinated lubricant forms a wrapping layer (or cloaking) on water droplets. Researchers tried to minimize this wrapping layer with ionic liquid [32] or mineral oil [33]. By adding asymmetric slippery bumps on the lubricated surface, the enhanced mass transport and droplet removal result in a dramatically increased condensation performance [33]. The liquid infused surfaces exhibit excellent droplet removal, but the hydrophobic nature remains on the surface and hinders nucleation. Furthermore, the liquid infused surfaces are flat, giving a small surface area for heat transfer.

An ideal surface to enhance condensation must have super-nucleation, rapid liquid-repellency, and large heat transfer areas. Therefore, the thread of this work is to design an ideal condensing surface, which must possess three characteristics: (i) hydrophilic surface for super-nucleation, (ii) boundary lubrication for condensate removal, and (iii) rough surface for heat transfer. Those three characteristics are needed on one surface to achieve the optimized condensation performance. By combining the micro/nanotextures of lotus leaves and the slippery surfaces of pitcher plants, we created the hydrophilic air-independent slippery rough surfaces (SRS) to enhance condensation (Fig. 1) [34,35]. The hydrophilic surface chemistry promotes nucleation, the slippery interface improves liquid repellency with air independence, and the rough surface provides a large surface-droplet contact for heat transfer. On conventional rough surfaces, droplets can be easily removed when they are partially floating on a layer of air (i.e., Cassie state), but can be highly pinned when they are in full contact with the rough surfaces (i.e., Wenzel state). On the slippery rough surfaces, droplets are mobile in the slippery Wenzel state owing to the boundary lubrication (Fig. 1). Such a slippery rough surface provides hydrophilic chemistry for nucleation, slippery interfaces for condensate removal, and large surface areas for heat transfer. However, the design rationale of such a condensing surface is not developed. In this work, we will theoretically study various parameters to increase heat transfer coefficients, providing theoretical principles for the surface design and optimization in condensation.

2. Results and discussion

2.1. Design rationale

To design an air-independent slippery rough surface, the solid surface must have two-tier roughnesses formed by hierarchical microtextures and nanotextures. Thus, we modified the surface chemistry with a hydrophobic coating on the entire surfaces, and then replaced the air lubricant within the nanotextures with liquid lubricant. The nanotextures could lock the liquid lubricant to form conformally lubricated microtextures. To this end, the surface chemistry, nanotextures, lubricant, and condensate liquid must follow the design principle of SLIPS [28,35]. This will ensure that the lubricant cannot be displaced by the condensate liquid (e.g., water). However, the lubricant between each microtexture was removed, so that the lubricated microtextures were in full contact with vapor in condensation. Furthermore, the surface chemistry

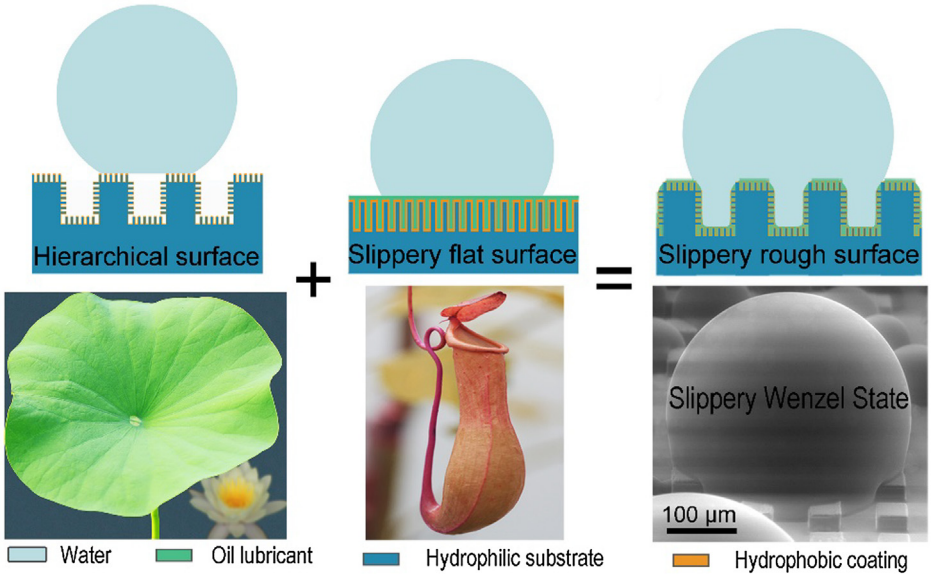

Fig. 1. Creating air-independent rough surfaces for liquid repellency [35].

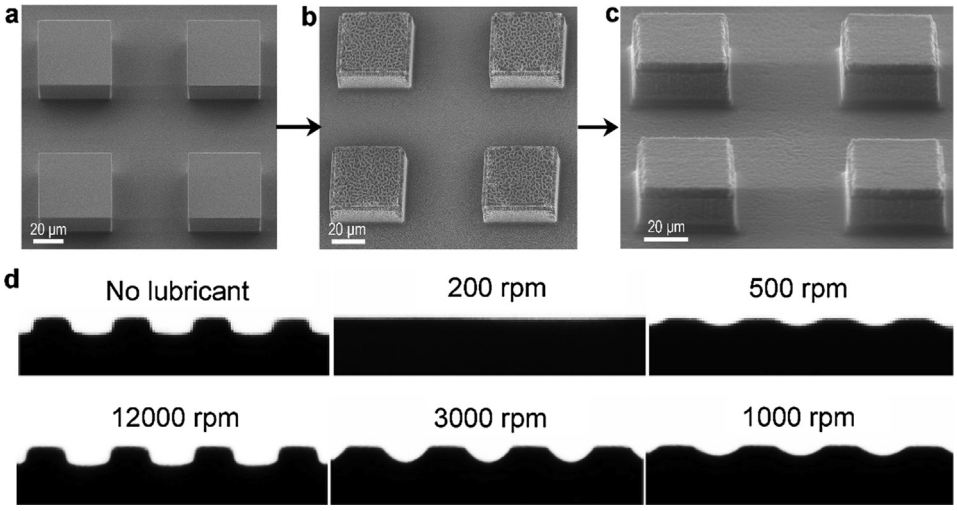

Fig. 2. Fabrication of air-independent slippery rough surfaces. (a) Silicon micropillars. (b) Nanotextured micropillars with a conformal silane coating. (c) Air-independent slippery rough surfaces. (d) Conformal lubrication with a spinner to remove the redundant liquid lubricant at different spin speeds (rpm).

and dimensions of the microtextures must be designed to ensure that the water droplet is in the Wenzel state. With the air-independence, the slippery Wenzel state can significantly increase the heat transfer areas. Since we were interested in the droplet mobility in the slippery Wenzel state, we carefully designed the dimensions of the micropillars based on the following correlation to ensure that the Wenzel state was more favorable than the Cassie state [6]:

$$cos\theta_c = \frac{\varphi - 1}{R_m - \varphi} \tag{1}$$

Here, θ_c is the critical CA. When the intrinsic CA of the lubricated flat surface $\theta < \theta_c$, the Wenzel state is more favorable than the Cassie state. The intrinsic CA θ is determined by the liquid lubricant, not the solid textures [34].

Air-independent wetting states can be the Wenzel state, hemiwicking state, and complete wetting state. To ensure the droplets are in the Wenzel state, the intrinsic CA θ cannot be too small because it may reach the hemiwicking state. Thus, the critical CA θ_h between the Wenzel state and hemiwicking state must meet the following relation [36]:

$$cos\theta_h = \frac{1 - \varphi}{R_m - \varphi} \tag{2}$$

Therefore, the surface chemistry and surface microstructures must follow the relation below:

$$\theta_h < \theta < \theta_c \tag{3}$$

2.2. Surface fabrication

To make such an air-independent slippery rough surface, we used deep reactive ion etching to make silicon micropillars (Fig. 2a). Then wet etching was used to make nanotextures everywhere (on the top and side walls of each micropillar as well as the bottom surface, Fig. 2b). Subsequently, trimethylchlorosilane (Sigma-Aldrich) was used to deposit a hydrophobic coating so that the micro/nanotextured surface can repel water. Finally, we displace the air within the nanotextures with liquid lubricant and ensure the liquid lubricant is infused within the nanotextures alone but not within the microtextures (Fig. 2c). To achieve that, we let the liquid lubricant fully cover the superhydrophobic micro/nanotextures. Then a spinner was used to remove the redundant liquid lubricant. When the spin speed is 12,000 rpm, the surface morphology showed conformally lubricated micropillars (Fig. 2c and d). The dimensions of slippery micropillars are: width 47 μm, length 53 μm, and height 19 μm.

2.3. Wetting characteristics

The apparent CAs of the droplets in the slippery Wenzel state are governed by the Wenzel's equation [35]:

$$Cos\theta^* = R_m cos\theta \tag{4}$$

where θ^* is the apparent CA on the air-independent slippery rough surfaces, R_m is the microscale roughness of the lubricated micropillars, and θ is the intrinsic CA on the slippery flat surface. We would like to further elaborate the surface chemistry and surface roughness on the SRS and SHS. On SRS, water cannot wet the solid surfaces directly as the lubricant cannot be displaced based on our design principle, so the surface chemistry is governed by the liquid lubricant, not the underneath solid chemical coating or solid structures. However, on SHS, the surface chemistry is governed by the chemical coating on the solid structures. On SRS, the roughness R_m is governed by the conformally lubricated microstructures. The nanostructures are completely covered by the liquid lubricant, so the nanoscale roughness r_n is not visible to water droplets. While on SHS, the roughness is determined by both the microstructures and nanostructures.

The equilibrium CA on the slippery flat surface (SFS) can be described by Young's equation [37]. Note that the lubricant thickness must be thin to avoid deformation. The thick lubricant will lead to the Neumann's wetting state. When there is no wrapping layer (or cloaking), the CA θ_1 is shown in Fig. 3a:

$$Cos\theta_1 = \frac{\gamma_{OW} - \gamma_{OG}}{\gamma_{WG}} \tag{5}$$

When certain lubricants are used (e.g., Krytox), a wrapping layer may exist on the water droplet [32]. Thus, the CA θ_2 for an oil-wrapped water droplet is shown in Fig. 3b:

$$Cos\theta_2 = \frac{\gamma_{OW} - \gamma_{OG}}{\gamma_{OW} + \gamma_{OG}} \tag{6}$$

However, the apparent CAs θ_1^* and θ_2^* follow the Wenzel's equation on the SRS. Therefore, the Eq. (4) remains valid no matter the wrapping layer exists or not (Fig. 3). The cloaking oil is unfavorable

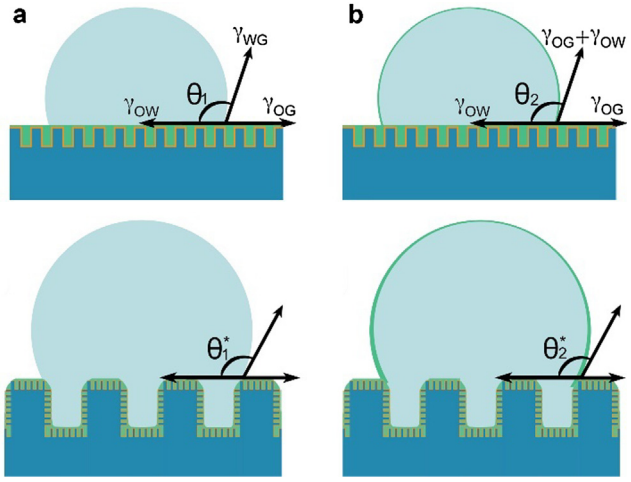

Fig. 3. Wetting characteristics on the slippery flat and rough surfaces. (a) Without wrapping layers, and (b) with wrapping layers on the water droplets.

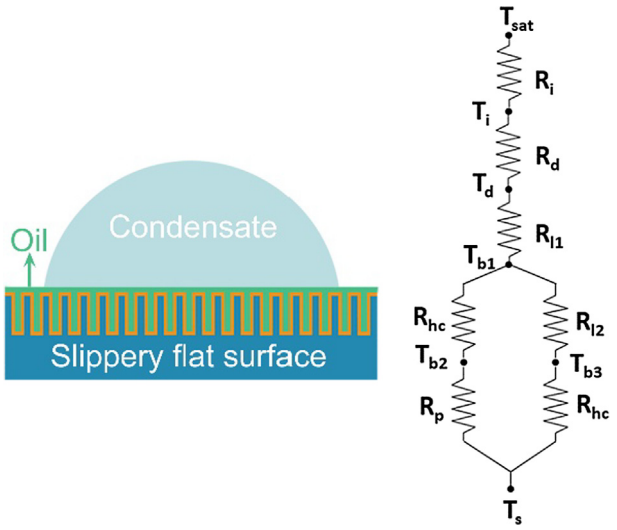

Fig. 4. Thermal resistance loop of dropwise condensation on the slippery flat surface. T_{sat} is saturated vapor temperature; T_i is the interfacial temperature on the droplet; T_d is the liquid temperature at the bottom of the droplet; T_{b1} is the lubricant temperature above the hydrophobic coating; T_{b2} is the temperature between the hydrophobic coating and the micro pillar; T_{b3} is the temperature between the lubricant and the hydrophobic coating; and T_s is the substrate temperature. R_i is the vapor-liquid interfacial thermal resistance. R_d, R_{l1}, R_{hc}, R_{l2}, and R_p are the thermal resistances of droplet, the lubricant above the micro pillars, the hydrophobic coating, the lubricant between the micro pillars, and the micro pillars, respectively.

for interfacial heat transfer, i.e., increase the interfacial thermal resistance. The nucleation tends to occur on a hydrophilic surface (or on —OH groups). Therefore, the cloaking oil with —CH_3 or —CF_3 groups will suppress nucleation [34].

The liquid infused surfaces with the lubricants of Krytox 101, mineral oil, and silicone oil show the contact angles (CAs, θ) of 121.5° ± 2.2°, 106.3° ± 2° and 104.1° ± 1.9°, respectively. Recently we have developed hydrophilic SFS with the CAs of 76.2° ± 2° and 57.2° ± 1.8° for hydroxy polydimethylsiloxane (PDMS, viscosity 25 cSt) and ionic liquid (1-butyl-3-methylimidazolium hexafluorophosphate, i.e., [bmim][PF_6]) [34]. The static CAs can approximately represent the advancing and receding CAs since all these slippery surfaces show the contact angle hysteresis (CAH, θ_{CAH}) below 5°. With this design principle, the surface chemistry can be changed by simply varying the lubricant. Therefore, we modeled the SFS using different lubricants to reach tunable CAs and compared their performances on heat transfer. We also modeled the SRS, on which the roughness is above 1, giving rise to larger heat transfer areas.

Since the surface chemistry is governed by the SFS (i.e., lubricated nanotextures), we will first build up the theoretical model of condensation on the SFS with tunable wettability. Once the condensation is well understood on the SFS (roughness $R_m = 1$), we will further study the condensation on the SRS (roughness $R_m > 1$). The air-independent SRS will circumvent the Cassie to Wenzel transition and surface flooding on SHS, providing a conceptually different strategy for condensation enhancement [34,35].

2.4. Modeling of condensation on SFS (roughness $R_m = 1$)

The slippery flat surface is made by replacing the air lubricant of the superhydrophobic nanotextures with water-immiscible oil lubricant (Fig. 4). We theoretically studied the heat transfer performance on the SFS by using the thermal resistance loop.

The equation for the heat transfer rate of an individual droplet q is shown in Eq. (7). In this equation, R is the radius of the growing droplet which is a variable. The first four terms in the denominator represent the liquid-vapor interface (R_i), droplet conduction (R_d), over-layer lubricant resistance (R_{l1}), and lubricant within the pillars (R_{l2}). The thermal resistances of the pillar and the hydrophobic coating are R_p and R_{hc}, respectively.

$$q = \frac{(\Delta T - \Delta Tc)\pi R^2}{\frac{1}{2h_i(1-\cos\theta)} + \frac{R\theta}{4k_w sin\theta} + \frac{\delta_l}{k_l sin^2\theta} + \left(\left(\left(\frac{\delta_{hc}}{\varnothing k_{hc} sin^2\theta} + \frac{H}{\varnothing k_p sin^2\theta}\right)^{-1} + \left(\frac{H}{(1-\varnothing)k_p sin^2\theta} + \frac{\delta_{hc}}{(1-\varnothing)k_{hc} sin^2\theta}\right)\right)^{-1}\right)^{-1}} \quad (7)$$

where R is the droplet radius, ΔT is the temperature difference between the saturated vapor and substrate temperature, $\Delta T_c = (T_{sat} - T_s)$ is the temperature drop due to the droplet curvature, δ_{hc}, δ_l, and H are the thickness of the hydrophobic coating, lubricant thickness, and pillar height, respectively. k_{hc}, k_l, k_w and k_p are the thermal conductivities of the hydrophobic coating, lubricant, water, and pillar, respectively. h_i is the interfacial condensation heat transfer coefficient from vapor-liquid phase change [8] and φ is the solid fraction.

The overall heat flux q'' can be obtained by the integration as shown below. Here, n(R) and N(R) are the population densities for small and large droplets before and after coalescence, respectively [8,38]. R_{min} is the initial radius when the droplet nucleates, and it is assumed to be 10 nm independent of the type of surface, R_e is the coalescence radius (assuming it is a half of the coalescence length), $\bar{R}$ is the departure radius that provides enough gravity for droplet departure [39], and τ is the droplet sweeping period.

$$q'' = \int_{R_{min}}^{R_e} qn(R)dR + \int_{R_e}^{\bar{R}} qN(R)dR \quad (8)$$

$$\text{Wheren(R)} = \frac{1}{3\pi R^2 \bar{R}}\left(R_e/\bar{R}\right)^{-2/3}\frac{R(R-R*)}{(R-R*)}\frac{A_2R+A_3}{A_2R_e+A_3} * \exp(X+Y) \quad (9)$$

$$X = \frac{A_2}{\tau * A_1}\left[\frac{{R_e}^2-R^2}{2} + R_{min}(R_e-R) - {R_{min}}^2\ln\left(\frac{R-R_{min}}{R_e-R_{min}}\right)\right] \quad (10)$$

$$Y = \frac{A_3}{\tau * A_1}\left[R_e - R - R_{min}\ln\left(\frac{R-R_{min}}{R_e-R_{min}}\right)\right] \quad (11)$$

$$A_1 = \frac{\Delta T}{h_{fg}\rho_w(1-cos\theta)^2(2+cos\theta)}$$

$$A_2 = \frac{\theta}{4k_w sin\theta}$$

$$A_3 = \frac{1}{2h_i(1-\cos\theta)} + \frac{\delta_l}{k_l sin^2\theta} + \left(\left(\left(\frac{\delta_{hc}}{\varnothing k_{hc} sin^2\theta} + \frac{H}{\varnothing k_p sin^2\theta}\right)^{-1} + \left(\frac{H}{(1-\varnothing)k_p sin^2\theta} + \frac{\delta_{hc}}{(1-\varnothing)k_{hc} sin^2\theta}\right)^{-1}\right)^{-1}\right)^{-1}$$

$$\tau = \frac{3{R_e}^2(A_2R_e+A_3)^2}{A_1\left(11A_2{R_e}^2 - 14A_2R_eR_{min} + 8A_3R_e - 11A_3R_{min}\right)} \quad (12)$$

$$N(R) = \frac{1}{3\pi R^2 \bar{R}}\left(R_e/\bar{R}\right)^{-2/3} \quad (13)$$

If N is the nucleation density and L_c is the coalescence length [38], then

$$Lc = 1/(4N)^{0.5} \quad (14)$$

The departure radius $\bar{R}$ can be calculated using the retention force equation [39]:

$$\rho gV = \sigma(\cos\theta_R - -\cos\theta_A)2\bar{R} \quad (15)$$

$$V = \frac{\pi(1-cos\theta)^2(2+cos\theta)\left(2\bar{R}\right)^3}{24sin^3\theta} \quad (16)$$

where θ_R is the receding CA, θ_A is the advancing CA and V is the volume of the droplet. We assume the surface is in the vertical orientation.

The thermal conductivities of liquid lubricants range from 0.09 W/m K to 0.15 W/m K, which are 246% and 477% higher than that of air. More importantly, the smaller CAH can dramatically increase the heat transfer coefficient at a constant CA (Fig. 5a). Specifically, when the CAH decreases from 16° to 2°, the heat transfer coefficient increases from 99.5 kW/m^2 K to 116.7 kW/m^2 K at the CA = 120°. The SFS can give small CAH (below 5°) with tunable wettability, with water CAs from 57.2° ± 1.8° to 121.5° ± 2.2°. Smaller CAs result in smaller thermal resistances across the liquid droplet. When the CA reduces from 120° to 57.2°, the heat transfer coefficient increases from 111.1 kW/m^2 K to 188.9 kW/m^2 K, showing a 70% enhancement (Fig. 5a). Therefore, the hydrophilic and slippery surface is favorable for condensation heat transfer. We refer to the experimental heat transfer coefficient in a prior publication [12], so in the theoretical study we assume 0.5% non-condensable gases as the reference shows. If there are more non-condensable gases, the heat transfer coefficient will decrease. The SRS are still based on surface modification, so they behave like other surfaces when non-condensable gases are present.

Heat is conducted through the lubricant and nanotextures parallelly. As the thermal conductivity of silicon is 144 W/m K, most of the heat will conduct through the silicon nanotextures. Thus, the lubricant locked within the nanotextures can provide the liquid-repellent function but will not reduce the heat transfer coefficient. However, there could be an over-layer lubricant above the nanotextures. It is shown that a 25 ± 5 nm lubricant film exists above the solid surface. Such a film is stabilized by van der Waals interactions between the liquid lubricant and solid surfaces [40]. This over-layer is super slippery for droplet removal. However, as the thickness of the over-layer lubricant δ_{l1} increases the thermal resistance also rises, resulting in decreased heat transfer performances (Fig. 5b). The heat transfer coefficient is not significantly reduced when δ_{l1} is below 20 nm. This overlayer can be easily removed because the nanotextures cannot retain it. On the SFS, we have taken the thickness of the over-layer lubricant as 1 nm in our model.

In the studies of jumping droplets, researchers assume that the droplet only jumps on superhydrophobic surfaces and the CAH is assumed to be negligible. However, CAH is an important parameter for droplets with low CAs. The droplet jumps when the jumping force dominates the retention force. On the SFS, we established a relationship between CAH and heat transfer coefficient and found that a lower CAH gave a better heat transfer performance at a constant CA. In this case, when the gravity force dominates the retention force in Eq. (15), the droplet starts to depart.

Our SFS shows the θ_{CAH} of 4°, indicating high mobility of the droplet. The CA can be simply tuned by changing the liquid

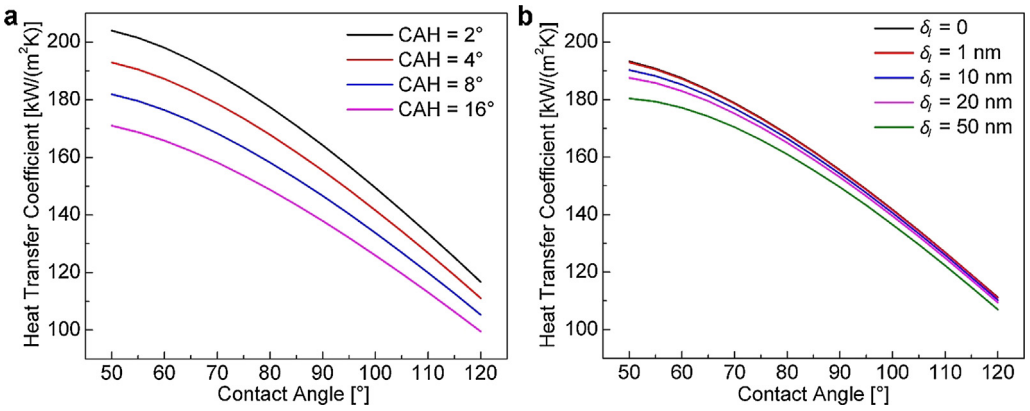

Fig. 5. Theoretical heat transfer coefficient on slippery flat surfaces. (a) Contact angle and contact angle hysteresis (R_e = 4 μm), and (b) the thickness of lubricant over layer (R_e = 4 μm, θ_{CAH} = 4°) influence heat transfer performances.

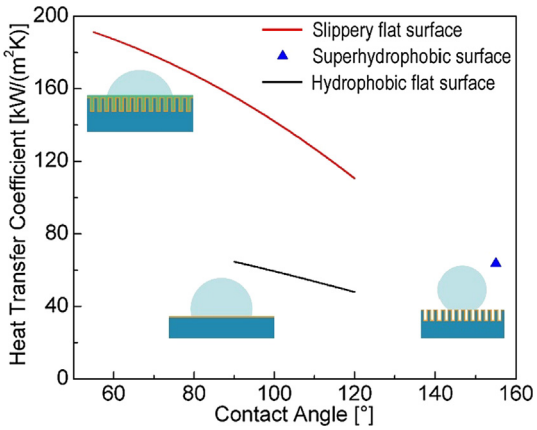

Fig. 6. Theoretical heat transfer coefficients on slippery flat surfaces with tunable wettability, superhydrophobic surface, and hydrophobic flat surface. On SFS, R_e = 4 μm, θ_{CAH} = 4°; on SHS, R_e = 2 μm; on hydrophobic flat surfaces, R_e = 10 μm, θ_{CAH} = 25°.

lubricant. Thus, the SFS shows a small CAH but tunable CAs, from 120° to 57.2°. However, when the surface textures and the hydrophobic coating is fixed, the SHS shows a fixed θ^* = 155°. The CAH on the hydrophobic flat surface is 25° [41]. The CAs can also be tuned by changing the hydrophobic coating. If we compare the SFS with the SHS and the hydrophobic flat surface, as shown in Fig. 6, the SFS (θ = 76.2°) shows the heat transfer coefficient of 172.5 kW/m^2 K, 286% larger heat transfer coefficient than that on the hydrophobic flat surface (θ = 120°, which is widely used) and 174% higher than to the SHS. Although the SFS shows both a high nucleation density and droplet mobility, it has smaller areas (roughness R_m = 1) which restrict its capability of nucleating more droplets.

When the gravitational force is larger than the retention force, the droplet will shed off. According to Eqs. (15) and (16), the departure radius is large for droplets with small CAs as the contact area becomes larger. In the prior model, it was assumed that the θ and θ_{CAH} were constant for various radii of droplets on SHS [9], so the smaller departure radius led to improved heat transfer performances (Fig. 7). However, on our SFS, the departure radius is a function of the intrinsic CA θ as shown in Eq. (15). A smaller CA θ results in a larger departure radius. Thus, the heat transfer coefficient is enhanced with the increasing departure radius. Note that Eq. (8) shows that a larger departure radius $\bar{R}$ favors the integration, resulting in a higher heat transfer coefficient. The theoretical heat flux is calculated by integrating the droplet size on the condensing surface. In a real condensation process, the droplet is removed, and then new droplets are nucleated. However, this theoretical model cannot consider the dynamics process with time. Sweeping droplets cannot be modeled here due to the complexity of different time steps. This is a limitation of the current theoretical model, which only shows the integration of all the droplets on the condensing surface at a given time but could not consider the re-nucleation of the next cycle.

When it reaches a critical value, the heat transfer coefficient decreases by increasing the departure radius (Fig. 7). The reason is that at higher contact angles the droplets have larger droplet height (increasing the circumference of the droplet) which increases the droplet conduction resistance and thus decreases the overall heat transfer coefficient. Since the departure radius is a function of contact angle, it varies from surface to surface. It is assumed that the departure radius varies at constant CA. For example, when we use Krytox oils with different viscosities as the lubricants, the contact angle hysteresis varies, but the contact angle will be constant.

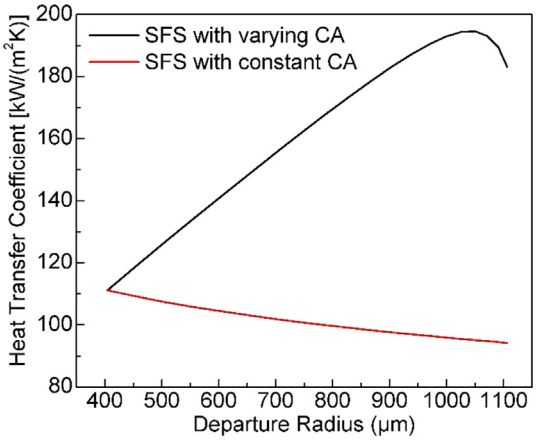

Fig. 7. The influence of departure radius on the heat transfer coefficient. The SFS with varying CA can be made by using a different type of lubricant. The SFS with constant CA can be made by changing the viscosity of the same type of lubricant (e.g., Krytox). Black curve: R_e = 4 μm, θ_{CAH} = 4°; red curve: R_e = 4 μm, θ_{CAH} = 4°, and θ = 120°. (For interpretation of the references to colour in this figure legend, the reader is referred to the web version of this article.)

2.5. Modeling of condensation on SRS (roughness $R_m > 1$)

On SHS, water droplets contact the top of each texture, but cannot be in full contact with the roughness. On SFS, water droplets are in contact with a slippery flat surface (R_m = 1). The heat transfer areas on both surfaces are small. To overcome the disadvantage of its small heat transfer areas, we created the slippery rough surfaces which combine the unique surface characteristics of pitcher plants and lotus leaves as shown in Fig. 1. The air-independent slippery rough surfaces are created by infusing liquid lubricant into the

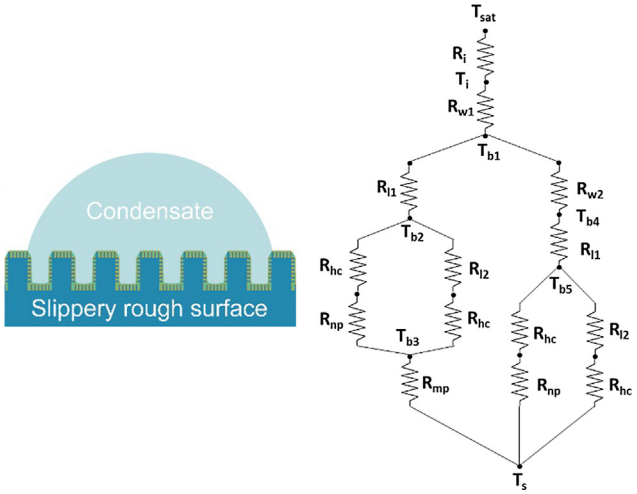

Fig. 8. Thermal resistance loop of dropwise condensation on the air-independent slippery rough surfaces. T_{sat} is saturated vapor temperature; T_i is the interfacial temperature on the droplet; T_{b1} is the lubricant temperature above the hydrophobic coating; T_{b2} is the temperature between the hydrophobic coating and the nanopillar; T_{b3} is the temperature between the nanopillar and the micropillar; T_{b4} is the temperature between water and the hydrophobic coating; T_{b5} is the temperature below the overlayer lubricant, and T_s is the substrate temperature. R_i and R_{w1}, R_{w2} are the thermal resistances of the vapor-liquid interface, the condensate droplet, and the condensate liquid within micropillars, respectively. R_{l1}, R_{hc}, R_{l2}, R_{np}, and R_{mp} are the thermal resistance of the lubricant above the nanopillars, the hydrophobic coating, the lubricant between the nanopillars, the nanopillars, and the micropillars, respectively.

nanostructures alone to increase the mobility of droplets even in the Wenzel state. The surface chemistry and slippery microtextures can be changed by varying the lubricant and surface roughness, respectively. Surface chemistry governs the intrinsic CA θ whereas surface structures amplify the apparent CA θ^*.

We modeled the SRS in a similar way using the thermal resistance loop (Fig. 8). The roughness of the slippery rough surface is given by the equation $R_m = 1 + 4wh/l^2$ where w is the width of the square micropillar with boundary lubrication, h is the height of the micropillar and l is the spacing between the micropillars. Due to the surface roughness, the apparent CA is governed by the Wenzel's equation (Eq. (4)).

The heat transfer rate q for an individual droplet is calculated in a similar way as that of the SFS, using thermal resistance loop. As shown in Eq. (17), $\varnothing_n$ and $\varnothing_m$ are the solid fractions of nanopillar and micropillar, and H_n and H_m are the heights of nanopillar and micropillar, respectively. The third term in the denominator represents the lubricant, hydrophobic coating, nanopillar, micropillar, and water thermal resistances (R_{l2}, R_{hc}, R_{np}, R_{mp}, R_{w2}), respectively.

$$q = (\Delta T - \Delta Tc)\pi R^2 * \left\{ \left(\frac{1}{2h_i(1-\cos\theta)} + \frac{R\theta}{4k_w sin\theta} + \left(\left(\left(\left(\frac{\delta_{hc}}{\varnothing_n * \varnothing_m * k_{hc} sin^2\theta} + \frac{H_n}{\varnothing_n * \varnothing_m * k_{np} sin^2\theta} \right)^{-1} + \left(\frac{H_n}{(1-\varnothing_n) * \varnothing_n * k_l sin^2\theta} + \frac{\delta_{hc}}{(1-\varnothing_n) * \varnothing_m * k_{hc} sin^2\theta} \right) \right)^{-1} + \frac{H_m}{\varnothing_m * k_{mp} sin^2\theta} + \frac{\delta_l}{\varnothing_m * k_l sin^2\theta} \right)^{-1} + \left(\left(\left(\frac{\delta_{hc}}{\varnothing_n * (1-\varnothing_m) * k_{hc} sin^2\theta} + \frac{H_n}{\varnothing_n * (1-\varnothing_m) * k_{np} sin^2\theta} \right)^{-1} + \left(\frac{H_n}{(1-\varnothing_n) * (1-\varnothing_m) * k_l sin^2\theta} + \frac{\delta_{hc}}{(1-\varnothing_n) * (1-\varnothing_m) * k_{hc} sin^2\theta} \right) \right)^{-1} + \frac{H_m}{(1-\varnothing_m) * k_w sin^2\theta} + \frac{\delta_l}{(1-\varnothing_m) * k_l sin^2\theta} \right)^{-1} \right)^{-1} \right\}^{-1} \tag{17}$$

Thus, the overall heat flux q'' is given by:

$$q'' = \int_{R_{min}}^{R_e} qn(R) * R_m dR + \int_{R_e}^{\bar{R}} qN(R) * R_m dR \tag{18}$$

The factor of roughness R_m is multiplied by the population densities of the small and large droplet to account for the increase in the droplet nucleation area on the slippery rough surface compared to the slippery flat surface.

On SRS, the effect of CAH on the heat transfer coefficient is like that on the SFS. A lower CAH results in a higher heat transfer coefficient because of the high droplet mobility (Fig. 9a). The condensed droplets are in full contact with the slippery rough surfaces. As demonstrated in our prior work, the retention force is proportional to the surface area of the slippery micropillars [35]. However, we have shown that the slippery microchannels can give a much smaller CAH than the slippery micropillars at a given roughness when the droplet slide in parallel with the slippery microchannels [34]. When the CAH is reduced from 16° to 2°, the higher heat transfer coefficient is increased by 19.3% at the roughness $R_m = 2$.

The lubricant retention is critical for the droplet repellency. On SRS, the lubricant is retained by the nanotextures. The height of nanopillars has little influence on the heat transfer coefficient (Fig. 9b). If the height of nanopillars is increased, we can retain more liquid lubricant within nanotextures for durable operations with almost no change in the heat transfer performance. Therefore, a larger height of the nanopillar can help retain lubricant and improve surface durability.

The roughness of the SRS can be increased either by increasing the height of the micropillars or decreasing the spacing between the micropillars. When the intrinsic CA is below 76°, the heat transfer coefficient increases from 172.3 kW/m^2 K to 323.6 kW/m^2 K, leading to an 87.8% enhancement. On the conventional slippery flat surface, the CA is 120°, so the heat transfer coefficient is 111.1 kW/m^2 K. When the roughness $R_m = 2$ and the intrinsic $\theta = 76°$, our SRS show a 191.3% higher heat transfer coefficient than the conventional slippery flat surface and a 407.2% higher heat transfer coefficient than SHS. The reason for the enhancement is that roughness reduces the apparent CA, and thus reduce the thermal resistance. Furthermore, the heat transfer areas are augmented. Both factors are favorable for heat transfer enhancement. Non-lubricated hydrophilic surfaces can also reduce the

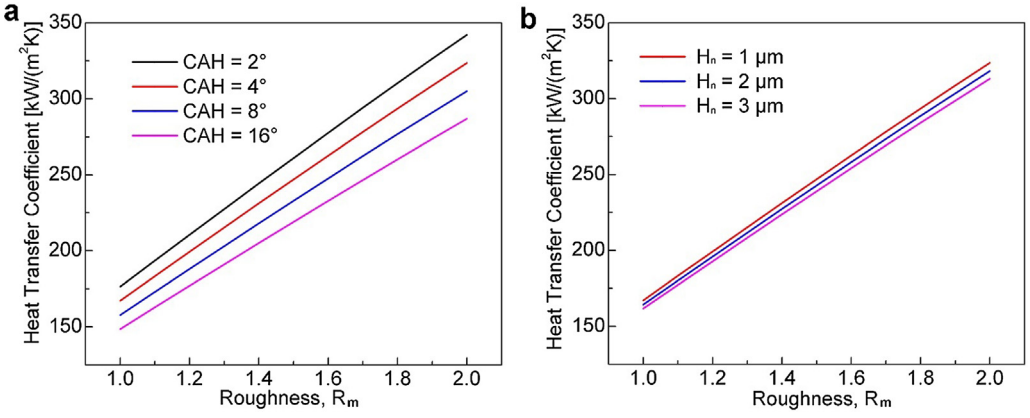

Fig. 9. Theoretical analysis of (a) CAH ($R_e = 4$ μm, $\theta = 76°$, and $H_n = 1$ μm) and (b) the height of nanopillars ($R_e = 4$ μm, $\theta = 76°$, and $\theta_{CAH} = 4°$) on condensation heat transfer.

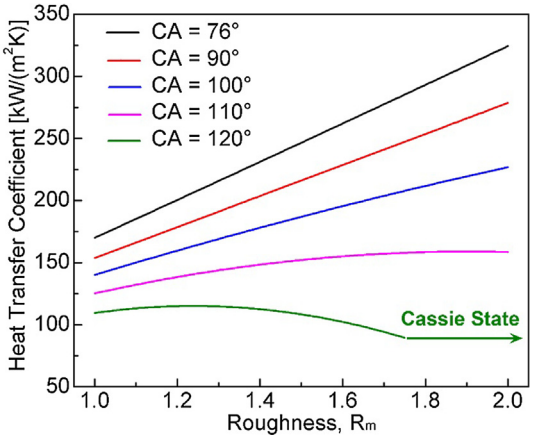

Fig. 10. Theoretical heat transfer coefficients of roughness-augmented condensation on air-independent rough surfaces (R_e = 4 μm, θ_{CAH} = 4°, and H_n = 1 μm). The CA is the intrinsic CA θ on SFS.

apparent CA by roughness, but the CAH on those surfaces is extremely high. Nonetheless, when the CA is above 90°, roughness increases the apparent CA. In the meantime, the heat transfer area is increased. There is a trade-off between the increased heat transfer area and the increased apparent CA. To ensure that the condensed droplets are in the Wenzel state, not the Cassie state, we used Eqs. (1) and (2) to set the restrictions for the roughness augmentation. When the intrinsic CAs are 120°, 110°, and 100°, the roughness R_m cannot be larger than 1.75, 2.44 and 4.57, respectively. Otherwise, the droplet will be in the Cassie state at a large roughness, which is out of the scope of this work (Fig. 10). For a higher intrinsic CA on the SFS (θ > 90°), as we increase the roughness R_m the apparent CA θ^* increases (Eq. (4)). This significantly increases the conduction thermal resistance (R_d) of the droplet, and thus decreases the heat transfer coefficient. The trade-off between the increased heat transfer area and the increased apparent CA exists when the intrinsic CA θ > 90° since the roughness increases the apparent CA (Fig. 10). This will increase the thermal resistance and decreases the contact area for heat transfer. The critical apparent CA is 151° when the intrinsic CA is 120°. However, as long as the slippery rough surface shows a small contact angle hysteresis in the Wenzel and hemiwicking state, there is no restriction with roughness when θ < 90°.

3. Conclusion

We experimentally fabricated the air-independent slippery rough surface on which the droplets are mobile in the slippery Wenzel state, and theoretically studied the design rationales for condensation heat transfer. To be clear, on a conventional rough surface the Wenzel state droplets cannot be completely removed from the surface textures, so the condensates will make the surface flooded even on superhydrophobic surfaces. The surface chemistry of our SRS is governed by the liquid lubricant, not the solid textures, and the roughness is determined by the lubricated microtextures. We first developed the slippery flat surface with tunable wettability by changing the lubricant. The hydrophilic SFS possess both high nucleation density and droplet mobility as compared to SHS, but still lack of heat transfer area. To solve this problem, we then developed the SRS by combining the slippery interfaces of pitcher plants and the rough textures of lotus leaves. Condensed droplets on our SRS are in the Wenzel state but can be effectively repelled because of the lubricated boundary conditions, and the roughness can increase the heat transfer areas. While SHS rely on the existence of air within the rough surface textures, we show that condensation on a rough surface can be significantly enhanced in the absence of air. Our theoretical models provide design rationales on various parameters, such as the design of slippery Wenzel state, lubricant thickness, the height of the pillars, roughness and the CAH. We also show that the condensation heat transfer coefficient on our SRS at the roughness R_m = 2 is 191.3% and 407.2% higher than those on the conventional slippery flat surface (θ = 120°) and SHS (θ^* = 155°), respectively. Compared with pure theoretical analysis, this theoretical study made reasonable assumptions based on the successful fabrication of the slippery rough surfaces. For example, we chose the contact angle of 76° as the hydrophilic slippery surface because this was achieved experimentally. Even though the slippery micropillars may get flooded during condensation, we point out that parallel slippery microchannels can repel condensates more effectively although the surface is temporally wetted [34]. Our theoretical studies gain significant insights into designing an air-independent surface for the enhancement of dropwise condensation.

Author contributions

X.D. conceived and supervised the research. X.D. designed and conducted the experiments. G.K.S., and X.D. carried out the theoretical modeling. G.K.S. and X.D. conducted the data analysis. G.K.S. and X.D. wrote and revised the paper.

Declaration of Competing Interest

The authors declare no conflict of interest.

Acknowledgment

The authors gratefully acknowledge the startup funding support by The University of Texas at Dallas, United States (UT Dallas), and National Science Foundation, United States (NSF) (Award No. 1929677). This project was partially funded by the Office of Research at UT Dallas through the Core Facility Voucher Program. G.K.S. acknowledges the discussion with Zongqi Guo and the teaching assistantship support from the Mechanical Engineering.

References

[1] H.J. Cho, D.J. Preston, Y. Zhu, E.N. Wang, Nanoengineered materials for liquid–vapour phase-change heat transfer, Nat. Rev. Mater. 2 (2016) 16092.
[2] D. Attinger, C. Frankiewicz, A.R. Betz, T.M. Schutzius, R. Ganguly, A. Das, C.-J. Kim, C.M. Megaridis, Surface engineering for phase change heat transfer: a review, MRS Energy Sustain. 1 (2014) E4.
[3] J.W. Rose, Dropwise condensation theory and experiment: a review, P. I. Mech. Eng. A-J. Pow. 216 (A2) (2002) 115–128.
[4] W. Barthlott, C. Neinhuis, Purity of the sacred lotus, or escape from contamination in biological surfaces, Planta 202 (1) (1997) 1–8.
[5] A.B.D. Cassie, S. Baxter, Wettability of porous surfaces, Trans. Faraday Soc. 40 (1944) 0546–0550.
[6] A. Lafuma, D. Quere, Superhydrophobic states, Nat. Mater. 2 (7) (2003) 457–460.
[7] J.B. Boreyko, C.-H. Chen, Self-propelled dropwise condensate on superhydrophobic surfaces, Phys. Rev. Lett. 103 (18) (2009) 184501.
[8] N. Miljkovic, R. Enright, E.N. Wang, Effect of droplet morphology on growth dynamics and heat transfer during condensation on superhydrophobic nanostructured surfaces, ACS Nano 6 (2) (2012) 1776–1785.
[9] R. Xiao, N. Miljkovic, R. Enright, E.N. Wang, Immersion condensation on oil-infused heterogeneous surfaces for enhanced heat transfer, Sci. Rep. 3 (2013) 1988.
[10] R. Wen, Q. Li, J. Wu, G. Wu, W. Wang, Y. Chen, X. Ma, D. Zhao, R. Yang, Hydrophobic copper nanowires for enhancing condensation heat transfer, Nano Energy 33 (2017) 177–183.
[11] Y. Li, D. Quéré, C. Lv, Q. Zheng, Monostable superrepellent materials, Proc. Natl. Acad. Sci. USA 114 (13) (2017) 3387–3392.
[12] R. Wen, S. Xu, X. Ma, Y.-C. Lee, R. Yang, Three-dimensional superhydrophobic nanowire networks for enhancing condensation heat transfer, Joule 2 (2) (2018) 269–279.

[13] A. Tuteja, W. Choi, M. Ma, J.M. Mabry, S.A. Mazzella, G.C. Rutledge, G.H. McKinley, R.E. Cohen, Designing superoleophobic surfaces, Science 318 (5856) (2007) 1618–1622.
[14] T. Liu, C.-J. Kim, Turning a surface superrepellent even to completely wetting liquids, Science 346 (6213) (2014) 1096–1100.
[15] X. Liu, P. Cheng, Dropwise condensation theory revisited: Part I. Droplet nucleation radius, Int. J. Heat Mass Transf. 83 (2015) 833–841.
[16] K. Rykaczewski, A.T. Paxson, M. Staymates, M.L. Walker, X. Sun, S. Anand, S. Srinivasan, G.H. McKinley, J. Chinn, J.H.J. Scott, K.K. Varanasi, Dropwise condensation of low surface tension fluids on omniphobic surfaces, Sci. Rep. 4 (2014) 4158.
[17] J. Boreyko, C.-H. Chen, Restoring superhydrophobicity of lotus leaves with vibration-induced dewetting, Phys. Rev. Lett. 103 (17) (2009) 174502.
[18] C. Lee, C.-J. Kim, Underwater restoration and retention of gases on superhydrophobic surfaces for drag reduction, Phys. Rev. Lett. 106 (1) (2011) 014502.
[19] S. Adera, R. Raj, R. Enright, E.N. Wang, Non-wetting droplets on hot superhydrophilic surfaces, Nat. Commun. 4 (2013) 2518.
[20] Y. Hou, M. Yu, X. Chen, Z. Wang, S. Yao, Recurrent filmwise and dropwise condensation on a beetle mimetic surface, ACS Nano 9 (1) (2015) 71–81.
[21] M.M. Derby, A. Chatterjee, Y. Peles, M.K. Jensen, Flow condensation heat transfer enhancement in a mini-channel with hydrophobic and hydrophilic patterns, Int. J. Heat Mass Transf. 68 (2014) 151–160.
[22] X. Chen, M.M. Derby, Combined visualization and heat transfer measurements for steam flow condensation in hydrophilic and hydrophobic mini-gaps, J. Heat Transfer 138 (9) (2016) 091503–091511.
[23] M. Alwazzan, K. Egab, B. Peng, J. Khan, C. Li, Condensation on hybrid-patterned copper tubes (I): characterization of condensation heat transfer, Int. J. Heat Mass Transf. 112 (2017) 991–1004.
[24] E. Ölçeroğlu, C.-Y. Hsieh, K.K.S. Lau, M. McCarthy, Thin film condensation supported on ambiphilic microstructures, J. Heat Transfer 139 (2) (2017), 020910–020910-020911.
[25] E. Ölçeroğlu, M. McCarthy, Self-organization of microscale condensate for delayed flooding of nanostructured superhydrophobic surfaces, ACS Appl. Mater. Interfaces 8 (8) (2016) 5729–5736.
[26] Y. Hou, M. Yu, Y. Shang, P. Zhou, R. Song, X. Xu, X. Chen, Z. Wang, S. Yao, Suppressing ice nucleation of supercooled condensate with biphilic topography, Phys. Rev. Lett. 120 (7) (2018) 075902.
[27] P.S. Mahapatra, A. Ghosh, R. Ganguly, C.M. Megaridis, Key design and operating parameters for enhancing dropwise condensation through wettability patterning, Int. J. Heat Mass Transf. 92 (2016) 877–883.
[28] T.-S. Wong, S.H. Kang, S.K.Y. Tang, E.J. Smythe, B.D. Hatton, A. Grinthal, J. Aizenberg, Bioinspired self-repairing slippery surfaces with pressure-stable omniphobicity, Nature 477 (7365) (2011) 443–447.
[29] A. Lafuma, D. Quéré, Slippery pre-suffused surfaces, Europhys. Lett. 96 (5) (2011) 56001.
[30] H.F. Bohn, W. Federle, Insect aquaplaning: nepenthes pitcher plants capture prey with the peristome, a fully wettable water-lubricated anisotropic surface, Proc. Natl. Acad. Sci. USA 101 (39) (2004) 14138–14143.
[31] M. Tenjimbayashi, R. Togasawa, K. Manabe, T. Matsubayashi, T. Moriya, M. Komine, S. Shiratori, Liquid-infused smooth coating with transparency, super-durability, and extraordinary hydrophobicity, Adv. Funct. Mater. 26 (37) (2016) 6693–6702.
[32] S. Anand, A.T. Paxson, R. Dhiman, J.D. Smith, K.K. Varanasi, Enhanced condensation on lubricant-impregnated nanotextured surfaces, ACS Nano 6 (11) (2012) 10122–10129.
[33] K.-C. Park, P. Kim, A. Grinthal, N. He, D. Fox, J.C. Weaver, J. Aizenberg, Condensation on slippery asymmetric bumps, Nature 531 (7592) (2016) 78–82.
[34] X. Dai, N. Sun, S.O. Nielsen, B.B. Stogin, J. Wang, S. Yang, T.-S. Wong, Hydrophilic directional slippery rough surfaces for water harvesting, Sci. Adv. 4 (3) (2018) eaaq0919.
[35] X. Dai, B.B. Stogin, S. Yang, T.-S. Wong, Slippery wenzel state, ACS Nano 9 (9) (2015) 9260–9267.
[36] J. Bico, U. Thiele, D. Quéré, Wetting of textured surfaces, Colloids Surf., A 206 (1–3) (2002) 41–46.
[37] T. Young, An essay on the cohesion of fluids, Philos. Trans. R. Soc. Lond. 95 (1805) 65–87.
[38] N. Miljkovic, R. Enright, E.N. Wang, Modeling and optimization of superhydrophobic condensation, J. Heat Transfer 135 (11) (2013) 111004–111014.
[39] C.G.L. Furmidge, Studies at phase interfaces. I. The sliding of liquid drops on solid surfaces and a theory for spray retention, J. Colloid Sci. 17 (4) (1962) 309–324.
[40] D. Daniel, J.V.I. Timonen, R. Li, S.J. Velling, J. Aizenberg, Oleoplaning droplets on lubricated surfaces, Nat. Phys. 13 (2017) 1020.
[41] A.T. Paxson, J.L. Yagüe, K.K. Gleason, K.K. Varanasi, Stable Dropwise Condensation for Enhancing Heat Transfer via the Initiated Chemical Vapor Deposition (iCVD) of Grafted Polymer Films, Adv. Mater. 26 (3) (2014) 418–423.